



### High-density monolithic pellets of double-sided graphene fragments based on zeolite-templated carbon

|                               |   |
|-------------------------------|---|
| Journal:                      | <i>Journal of Materials Chemistry A</i>   |
| Manuscript ID                 | TA-COM-11-2020-011625.R3  |
| Article Type:                 | Communication   |
| Date Submitted by the Author: | 12-Mar-2021   |
| Complete List of Authors:     | Gabe, Atsushi; Tohoku University, Institute of Multidisciplinary Research for Advanced Materials<br>Ouzzine, Mohammed; Tohoku University, Institute of Multidisciplinary Research for Advanced Materials<br>Taylor, Erin; Montana State University Bozeman<br>Uchiyama, Naoki; Atsumitec CO., Ltd.<br>Stadie, Nicholas; Montana State University Bozeman, Department of Chemistry & Biochemistry<br>Kanai, Tomomi; Atsumitec CO., Ltd.<br>Nishina, Yuta; Okayama University, Research Core for Interdisciplinary Sciences<br>Tanaka, Hideki; Shinshu University, Research Initiative for Supra-Materials<br>Pan, Zheng-Ze; Tohoku University, Advanced Institute for Materials Research, Tohoku University<br>Kyotani, Takashi; Tohoku University, Institute of Multidisciplinary Research for Advanced Materials<br>Nishihara, Hiroto; Tohoku University, Institute of Multidisciplinary Research for Advanced Materials |
|                               |   |

## COMMUNICATION

## High-density monolithic pellets of double-sided graphene fragments based on zeolite-templated carbon

Received 00th January 20xx,  
Accepted 00th January 20xx

DOI: 10.1039/x0xx00000x

Atsushi Gabe,<sup>a</sup> Mohammed Ouzzine,<sup>ab</sup> Erin E. Taylor,<sup>c</sup> Nicholas P. Stadie,<sup>c</sup> Naoki Uchiyama,<sup>d</sup> Tomomi Kanai,<sup>d</sup> Yuta Nishina,<sup>e</sup> Hideki Tanaka,<sup>f</sup> Zheng-Ze Pan,<sup>g</sup> Takashi Kyotani,<sup>a</sup> Hiroto Nishihara<sup>\*ag</sup>

**High-density and highly porous graphene-based pellets that exhibit an anomalous gas densification property have been fabricated by using zeolite-templated carbon (ZTC) as the major component and reduced graphene oxide (rGO) as a pure carbon binder. The unique structure of each ZTC particle consists of double-sided graphene fragments connected in a periodic, three-dimensional framework. The graphene-like sheets of rGO strongly connect the ZTC particles upon hot-pressing via the generation of a large amount of unpaired electron spins, yielding monolithic pellets with exceptional mechanical toughness. The uniaxial pressing applied to the isotropic ordered framework of ZTC during pelletization leads to unique anisotropic structures. The so-obtained pellets represent a high density packing of graphene nanofragments with high volumetric surface area that exhibits high volumetric H<sub>2</sub> storage at room temperature.**

As a response to global climate change, considerable efforts have been made to develop energy storage and conversion systems that do not emit greenhouse gases.<sup>1</sup> One of the key efforts is the development of porous materials for efficient and effective energy storage and supply<sup>2</sup> in applications such as in gaseous fuel storage,<sup>3,4</sup> electrochemical energy storage,<sup>5,6</sup> and heat pumps.<sup>7</sup> The energy storage capacity derived from interfacial adsorption on a porous material increases with

increasing surface area. Additionally, in practical applications where a compact design is required, the volumetric performance is more important than the gravimetric performance.<sup>8</sup> Thus, volumetric surface area,  $S_v$  [m<sup>2</sup> cm<sup>-3</sup>], is of greater importance than gravimetric surface area,  $S_g$  [m<sup>2</sup> g<sup>-1</sup>], in assessing candidate porous materials for mobile energy storage. The preparation of high-density carbon pellets with large  $S_v$  has been reported by densification<sup>9-11</sup> of zeolite-templated carbon (ZTC)<sup>8</sup> which comprises atomically thin (double-sided) nanographene walls and has an extremely high gravimetric surface area of ca. 4000 m<sup>2</sup> g<sup>-1</sup>.<sup>12</sup> However, self-standing pellets made solely from ZTC are not mechanically very robust, restricting their practical applications. In this work, high-density pellets with high volumetric surface area and glass-like hardness which enables easy handling<sup>13</sup> are prepared by the compaction of two types of graphene-based materials. The major component is ZTC, combined with a minor component of reduced graphene oxide (rGO) as a pure carbon binder.<sup>14</sup> This unique graphene-graphene compositing strategy, benefitting from both rational size-matching of the two components and the unique mechanical properties of ZTC and rGO, results in the formation of highly robust monolithic pellets with extraordinary gas densification property toward N<sub>2</sub> and high volumetric H<sub>2</sub> storage.

In preliminary experiments, we examined the thermal reduction behaviour of graphene oxide (GO) toward better understanding its applications as a binder for porous carbon particulate materials such as ZTC. Thermal gravimetry (TG) of the pristine GO (Fig. S1) under helium revealed that the thermal decomposition of GO begins at 120 °C and completes at 300 °C, as confirmed by X-ray diffraction (XRD) performed before and after heat treatment (Fig. S2). The intense XRD peak at 10.1° corresponding to the inter-sheet distance of 0.87 nm of pristine GO shifts to 12.2° after heat treatment at 160 °C (just above the onset temperature observed in TG), indicating a decrease in the inter-sheet distance to 0.72 nm. Upon heat treatment at 300 °C, the intense GO peak shifts to 24.2° (inter-sheet distance of 0.37 nm) which is typical of reduced GO

<sup>a</sup> Institute of Multidisciplinary Research for Advanced Materials, Tohoku University, 2-1-1, Katahira, Aoba-ku, Sendai, 980-8577, Japan.

<sup>b</sup> Department of Chemistry, Multidisciplinary Faculty of Beni-Mellal, University of Sultan Moulay Slimane, Av. Mghila, BP 592, 23000, Beni-Mellal, Morocco

<sup>c</sup> Department of Chemistry & Biochemistry, Montana State University, Bozeman, Montana, 59717, United States

<sup>d</sup> Atsumitec CO., Ltd. 7111, Yuto-cho, Nishi-ku, Hamamatsu-shi, Shizuoka 431-0192, Japan

<sup>e</sup> Research Core for Interdisciplinary Sciences, Okayama University, Tsushimanaka, Kita-ku, Okayama 700-8530, Japan

<sup>f</sup> Research Initiative for Supra-Materials (RISM), Shinshu University, 4-17-1 Wakasato, Nagano 380-8553, Japan.

<sup>g</sup> Advanced Institute for Materials Research, Tohoku University, 2-1-1, Katahira, Aoba-ku, Sendai, 980-8577, Japan.

Electronic Supplementary Information (ESI) available: e: Experimental section and supplementary figures. See DOI: 10.1039/x0xx00000x

(rGO). When GO is heated under applied pressure (i.e., hot-pressed), the reduction proceeds more favourably, as shown in Fig. S3. Therefore, GO can be thermally transformed into rGO during pelletization conditions explored in this work.

High-density pellets consisting of efficiently packed graphene fragments accessible by a three-dimensional network of micropores were prepared through the hot-pressing of ZTC together with in-situ-reduced GO. The initial weight ratio of ZTC and GO was 95:5. Details as to the preparation procedure can be found in the Electronic Supplementary Information (ESI). In naming the pellets, the pressure and temperature during the hot-pressing step are indicated after the prefix ZTC\_rGO (e.g., ZTC\_rGO\_T300\_P345 indicates hot-pressing at a maximum temperature of 300 °C and a pressure of 345 MPa). A representative photograph of a single monolithic pellet (ZTC\_rGO\_T160\_P345) is shown in an inset of Fig. 1. The resulting pellets are mechanically sturdy with glass-like texture (see the supplemental movie) and not easily broken down into powder upon handling, unlike conventional activated carbon pellets prepared in similar conditions. In the absence of GO as a binder, a well-shaped pellet of ZTC could not be obtained under most conditions (the best such result is referred to as ZTC\_T160\_P145), demonstrating the importance of GO as an effective binder in the densification of ZTC.

Considering the fact that hot-pressing of ZTC without rGO cannot yield mechanically rigid pellets, there is a possibility of the formation of covalent bonds between ZTC and rGO or between rGO itself by recombination of radicals generated during hot-pressing. Such a recombination of radicals is known to occur, for example, at the rubber/carbon interface<sup>15</sup> and polymer/graphene interface.<sup>16</sup> To evaluate this assumption, the quantity of radicals (unpaired electron spins) in a representative pellet, ZTC\_rGO\_T160\_P345, was measured by electron spin resonance (ESR) spectroscopy (Fig. 1).<sup>17</sup>

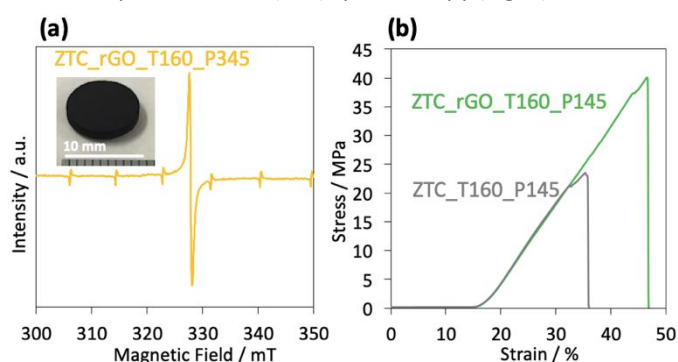


Fig. 1. (a) Photograph and ESR spectrum of a representative densified monolith of ZTC and rGO prepared by hot-pressing at 160 °C and 345 MPa (ZTC\_rGO\_T160\_P345). (b) Stress-strain curves of ZTC\_rGO\_T160\_P145 and ZTC\_T160\_P145.

As indicated by a pair of sharp peaks around 328 mT, the pellet was found to include a large number of unpaired spins ( $9.2 \times 10^{15} \text{ g}^{-1}$ ). An even larger number of unpaired spins were detected in a pellet prepared at a higher temperature (ZTC\_rGO\_T300\_P345):  $1.5 \times 10^{16} \text{ g}^{-1}$  (Fig. S4). On the other hand, both ZTC and GO have far fewer unpaired spins prior to

pelletization ( $3.3 \times 10^{15} \text{ g}^{-1}$  and  $1.7 \times 10^{15} \text{ g}^{-1}$ , respectively), and these values do not greatly change with rising temperature (Fig. S5 and S6). These results suggest that the radicals are formed due to the cleavage of chemical bonds or formation of other defects within the ZTC and rGO structures during hot-pressing. It is reasonable that some of these radicals would be recombined during the formation of the mechanically robust and high-density pellets. Of the remaining radicals, those which exist at accessible sites to air should be quenched, while the radicals located deeper within the ZTC particle cores would still remain isolated from the air and could therefore be detected by ESR. Thus, the larger amount of unpaired spins detected in the hot-pressed samples serves as indirect evidence for the generation of radicals upon hot-pressing.

The mechanical effect of the rGO binder on the ZTC monoliths was further investigated by compression testing. The stress-strain curves of two pellets, with (ZTC\_rGO\_T160\_P145) and without (ZTC\_T160\_P145) rGO binder, are compared in Fig. 1b. While the two samples show a similar slope (therefore a similar Young's modulus), the fracture strength of ZTC\_rGO\_T160\_P145 (40.1 MPa) is much larger than that of ZTC\_T160\_P145 (23.5 MPa) and other graphene-based monoliths reported elsewhere,<sup>18</sup> demonstrating the remarkable effect of the rGO binder on the improvement of mechanical strength in the monoliths prepared herein.

Scanning electron microscopy (SEM) images of the hot-pressed ZTC monoliths with (ZTC\_rGO\_T160\_P145) and without (ZTC\_T160\_P145) rGO binder are shown in Fig. 2. Without rGO, the surface of the resulting sample is rough (Fig. 2a) and there are obvious inter-particle voids at higher magnification (Fig. 2b) indicating that the ZTC particles (ca. 200 nm in size) are not densely packed. By contrast, the cross-section of ZTC\_rGO\_T160\_P145 shows a very dense structure without the presence of large voids (Fig. 2c). At higher magnification (Fig. 2d), the ZTC particles are observed to be neatly "wrapped" by the rGO binder and therefore connected together in highly densified structures. The success of such "wrapped" composites of ZTC (ca. 200 nm) and rGO (ca. 1  $\mu\text{m}$ ) seems to depend on the effective size matching of the two materials to promote dense and intimate packing.

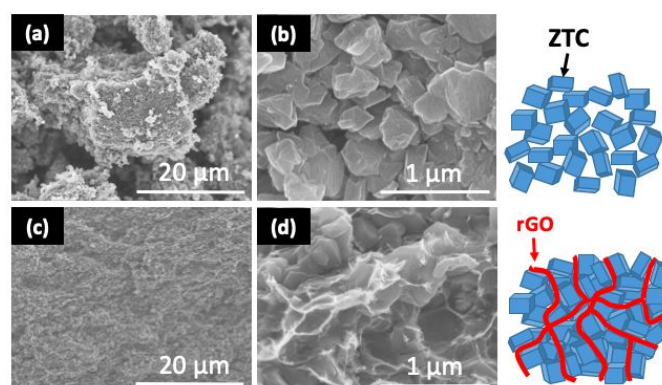


Fig. 2. SEM images of (a,b) ZTC\_T160\_P145 (top-view) and (c,d) ZTC\_rGO\_T160\_P145 (cross-section) at (a,c) low and (b,d) high magnification. Inset illustrations show the difference in micro-

morphologies of the pellets produced with and without rGO (red).

Indeed, the same preparation technique was not successful for densifying commercial activated carbon (MSC-30, Kansai Coke and Chemicals Co. Ltd.) instead of ZTC (Fig. S7), likely because of the mismatch in particle size between the activated carbon ( $> 10 \mu\text{m}$ ) and rGO (ca.  $1 \mu\text{m}$ ).

While pristine ZTC has an isotropic ordered structure derived from its cubic zeolite template,<sup>19</sup> unidirectional hot-pressing likely induces anisotropy in the structure of the resulting densified ZTC pellets. To investigate this phenomenon, X-ray diffraction (XRD) was measured on two different aspects of a series of pellets prepared at  $160 \text{ }^\circ\text{C}$ : incident upon the pressed surface (Fig. 3a) and incident upon the cross-section (Fig. 3b). The pristine ZTC powder exhibits a sharp reflection at  $2\theta = 6.4^\circ$  corresponding to the (111) planes of the zeolite NaY template.<sup>20</sup> While the ordered structure is lost above  $145 \text{ MPa}$  in Fig. 3a, the ordered structure remains even at  $345 \text{ MPa}$  in Fig. 3b, indicating the formation of an anisotropic structure. The results of Fig. 3a and 3b are schematically summarized in Fig. 3c. Upon hot-pressing, the diffraction planes parallel to the pressing direction are retained, while the diffraction planes perpendicular to the pressing direction are destroyed. This anisotropy is evident not only in the ZTC ordered structure, but also in the GO stacking structure. Similar effects were also observed at higher temperature ( $300 \text{ }^\circ\text{C}$ , Fig. S8). Detailed discussion of this result is given in the Supplementary Information. It was also confirmed that these anisotropic properties disappear when the pellet is broken down into powder (Fig. S9).

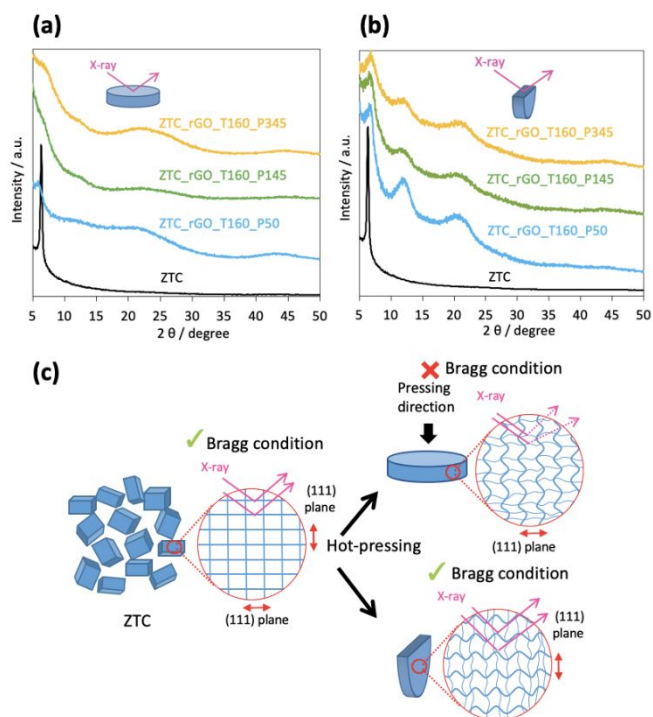


Fig. 3. XRD patterns incident to (a) the pressed surface and (b) the cross-section of ZTC/rGO pellets prepared at  $160 \text{ }^\circ\text{C}$  and a series of increasing pressure. The XRD pattern of pristine ZTC powder (black) is shown for reference. (c) Schematic depiction

of the effects of pelletization on the isotropic structure of ZTC, as revealed by XRD.

The porosity and surface area of the ZTC pellets were investigated by measurements of  $\text{N}_2$  adsorption/desorption isotherms at  $-196 \text{ }^\circ\text{C}$ , in comparison to pristine ZTC. In Fig. 4a, Pristine ZTC powder exhibits a type I isotherm by the IUPAC classification, arising from its uniform micropores ( $1.2 \text{ nm}$  in width)<sup>19</sup> arranged in an ordered network, showing almost no mesoporosity or larger pores. Upon hot-pressing, the general type I shape is preserved and the pore volume decreases with increasing temperature and pressure. The logarithmic plot (Fig. 4b) shows that  $\text{N}_2$  adsorption in the low pressure range of  $P/P_0 < 10^{-4}$  increases with temperature and pressure, suggesting the pore narrowing of ZTC upon hot-pressing.<sup>9</sup> The pore narrowing is indeed confirmed by the pore-size distributions which were calculated by a non-local density functional theory (NLDFT) method using  $\text{N}_2$  adsorption data (Fig. 4c).

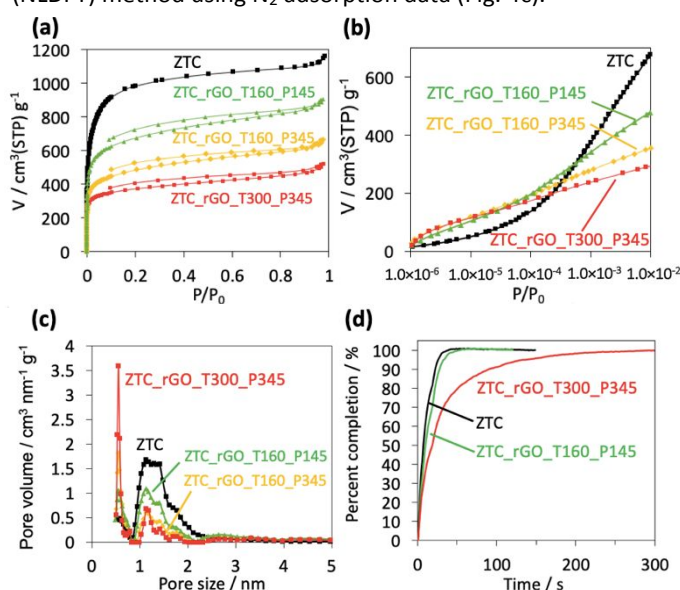


Fig. 4. (a,b)  $\text{N}_2$  adsorption/desorption isotherms at  $-196 \text{ }^\circ\text{C}$  on ZTC/rGO pellets, plotted as a function of (a) normal and (b) logarithmic partial pressure. In (b), only the range below  $P/P_0 = 0.01$  is shown. The adsorption isotherm on pristine ZTC powder (black) is shown for reference. (c) Pore-size distributions (NLDFT, slit-pore model). (d)  $\text{CO}_2$  adsorption kinetics at  $25 \text{ }^\circ\text{C}$  for  $300 \text{ s}$  at  $300 \text{ Pa}$  on ZTC and ZTC/rGO pellets.

The textural properties (surface area and pore volume) and densities of the ZTC pellets are summarized in Table 1. With increasing temperature and pressure of hot-pressing, the pellet density ( $\rho_{\text{bulk}}$ ) increases while the gravimetric surface area ( $S_g$ ) and total pore volume ( $V_{\text{total}}$ ) decrease. Note that  $V_{\text{total}}$  is defined here as the volume of pores that are less than  $50 \text{ nm}$ . Such a tendency follows expected trends for the compaction of porous materials. The volumetric surface area ( $S_v$ ) first increases and then decreases with increasing temperature and pressure; the maximum occurs when the particle compaction and subsequent decline of  $S_g$  are well

balanced, at  $1732 \text{ m}^2 \text{ cm}^{-3}$  in ZTC\_GO\_T160\_P145. This volumetric surface area is higher than previously reported value in the literature (representative examples are summarized in Table S1).

Table 1 Pore structure and density of pristine ZTC and ZTC/rGO pellets.

| Sample            | $S_g^a/$<br>$\text{m}^2 \text{ g}^{-1}$ | $\rho_{\text{bulk}}^b/$<br>$\text{g cm}^{-3}$ | $\rho_{\text{max}}^c/$<br>$\text{g cm}^{-3}$ | $\rho_{\text{skel}}^d/$<br>$\text{g cm}^{-3}$ | $V_{\text{total}}^e/$<br>$\text{cm}^3 \text{ g}^{-1}$ | $S_v^f/$<br>$\text{m}^2 \text{ cm}^{-3}$ |
|-------------------|---|---|--|---|---|--|
| ZTC               | 3806                                    | 0.17  | 0.44   | 1.80  | 1.74  | 647                                      |
| ZTC_T160_P145     | 3110                                    | 0.16  | 0.48   | n.m. <sup>g</sup>                             | 1.54  | 498                                      |
| ZTC_rGO_T160_P50  | 2685                                    | 0.52  | 0.51   | 1.73  | 1.43  | 1396                                     |
| ZTC_rGO_T160_P145 | 2585                                    | 0.67  | 0.51   | 1.66  | 1.35  | 1732                                     |
| ZTC_rGO_T160_P345 | 1831                                    | 0.83  | 0.66   | 1.74  | 1.00  | 1520                                     |
| ZTC_rGO_T300_P50  | 2486                                    | 0.52  | 0.51   | 1.78  | 1.31  | 1293                                     |
| ZTC_rGO_T300_P145 | 2248                                    | 0.75  | 0.57   | 1.64  | 1.16  | 1686                                     |
| ZTC_rGO_T300_P345 | 1450                                    | 0.98  | 0.74   | 1.70  | 0.76  | 1421                                     |

<sup>a</sup> Surface area as determined by the BET method between  $P/P_0 = 0.01$ - $0.05$ .

<sup>b</sup> Bulk density as determined from the pellet weight and hand-measured pellet volume.

<sup>c</sup> Maximum density as determined by Eqn. (1).

<sup>d</sup> Skeletal density as determined by He pycnometry.

<sup>e</sup> Total pore volume as determined from the  $\text{N}_2$  adsorption amount at  $P/P_0 = 0.96$ .

<sup>f</sup> Volumetric surface area as determined from  $S_g$  and  $\rho_{\text{bulk}}$ .

<sup>g</sup> Not measured.

The gas adsorption kinetics within the ZTC monoliths were evaluated by measuring the time until completion<sup>21</sup> of  $\text{CO}_2$  adsorption at  $25^\circ\text{C}$  (Fig. 4d). While the adsorption rate within ZTC\_rGO\_T300\_P345 is the lowest, gas uptake occurs in ZTC\_rGO\_T160\_P145 at a comparable rate to that of the pristine ZTC, indicating that the fast diffusion path of ZTC<sup>22</sup> is well retained in ZTC\_rGO\_T160\_P145.

From the textural properties presented in Table 1, it appears that the  $\rho_{\text{bulk}}$  values determined by hand measurements of the pellet weight and volume are anomalously high. For comparison, the theoretical maximum density ( $\rho_{\text{max}}$ ) can instead be calculated from  $V_{\text{total}}$  and the skeletal density ( $\rho_{\text{skel}}$ ) as follows:

$$\rho_{\text{max}} = \frac{1}{1/\rho_{\text{skel}} + V_{\text{total}}} \quad (1)$$

Owing to its dependence on  $V_{\text{total}}$  (determined by  $\text{N}_2$  adsorption measured at  $-196^\circ\text{C}$ ),  $\rho_{\text{max}}$  does not take large pores ( $> 50 \text{ nm}$ ) into consideration.<sup>8</sup> Generally, porous pellets contain pores larger than  $50 \text{ nm}$ , and therefore,  $\rho_{\text{bulk}}$  should be smaller than  $\rho_{\text{max}}$ . However, the  $\rho_{\text{bulk}}$  values for all ZTC/rGO pellets exceed their corresponding values for  $\rho_{\text{max}}$ . Thus, the  $\rho_{\text{max}}$  of the pellets is apparently underestimated. The detailed discussion as to the possible reasons is given in the Supplementary Information where we have considered the effect of underestimation of  $\rho_{\text{skel}}$  and overestimation of  $V_{\text{total}}$  because of the significant adsorption-induced expansion in ZTC.<sup>7</sup> However, the noticeable deviation of  $\rho_{\text{bulk}}$  from  $\rho_{\text{max}}$  cannot be explained only by these effects. A remaining

possibility is that the density of  $\text{N}_2$  confined within the narrow pores of the ZTC/rGO pellets is higher than the density of liquid  $\text{N}_2$  ( $0.808 \text{ g cm}^{-3}$ ). It is found that the density of the adsorbed nitrogen at  $-196^\circ\text{C}$  and  $P/P_0 = 0.96$  would need to be estimated at least as  $0.98 \text{ g cm}^{-3}$ . This value is comparable to the density of solid  $\text{N}_2$  ( $1.03 \text{ g cm}^{-3}$ ), indicating the enormous magnitude of densification of molecular adsorbates which can be caused by freezing point depression of  $\text{N}_2$ <sup>23</sup> within the high density yet highly porous graphene-like pellets achieved in the present work.

To demonstrate an advantage of their anomalous gas densification properties toward applications in energy storage, the  $\text{H}_2$  storage capacity of ZTC\_rGO\_T160\_P145 at  $25^\circ\text{C}$  was compared with the pristine ZTC powder. The excess adsorption uptake of  $\text{H}_2$  ( $M_{\text{excess}}$  [wt%]) on both materials up to 100 bar at room temperature is shown in Fig. 5a. The excess gravimetric uptake on ZTC\_rGO\_T160\_P145 is lower than that on pristine ZTC owing to a reduction in surface area upon hot-pressing. However, toward practical applications, the volumetric total storage amount ( $W_{\text{total}}$  [ $\text{g L}^{-1}$ ]) calculated by  $W_{\text{total}} = (M'_{\text{excess}} + M_{\text{gas}}) \times 1000\rho_{\text{bulk}}$ <sup>24</sup> is a more important metric of performance, where  $M'_{\text{excess}}$  is the surface excess amount expressed with the unit of  $\text{g g}^{-1}$  [ $M'_{\text{excess}} = M_{\text{excess}}/(100 - M_{\text{excess}})$ ].  $M_{\text{gas}}$  [ $\text{g g}^{-1}$ ] is the amount of compressed  $\text{H}_2$  within the micro/mesopore network (See ESI for the calculation of  $M_{\text{gas}}$ ). The total volumetric hydrogen capacity of ZTC\_rGO\_T160\_P145 and pristine ZTC powder at  $25^\circ\text{C}$  up to 100 bar are shown in Fig. 5b. The ZTC monolith stores  $>2\times$  the amount of  $\text{H}_2$  per unit volume at all pressures up to 100 bar. For comparison, physisorption-based  $\text{H}_2$  storage values reported in porous pellets are summarized in Table S2. The reported  $W_{\text{total}}$  values at  $25^\circ\text{C}$  and 100 bar are the range of  $3.2$  to  $11.2 \text{ g L}^{-1}$ . The ZTC pellet exhibits large  $W_{\text{total}}$  value ( $10.5 \text{ g L}^{-1}$ ) which is comparable to the best values reported in porous carbon pellets ( $11$  and  $11.2 \text{ g L}^{-1}$ ).<sup>25,26</sup> These results demonstrate a good hydrogen storage performance of the ZTC pellets.

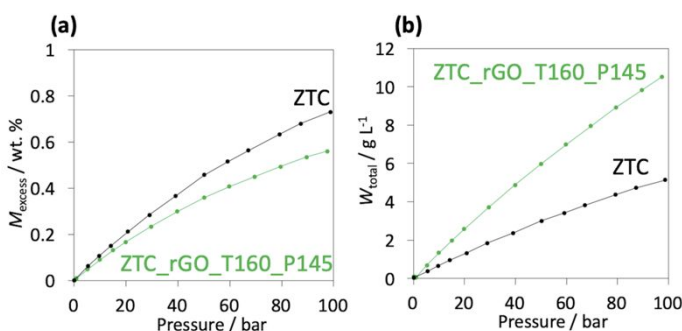


Fig. 5. Excess and total  $\text{H}_2$  storage capacity of ZTC and ZTC\_rGO\_T160\_P145 at  $25^\circ\text{C}$ . (a) Surface excess amount. (b) Total storage amount.

In summary, mechanically robust and high-density graphene-like pellets can be fabricated by a graphene-graphene compositing strategy based on ZTC as an ordered porous particulate and rGO as a size-matched binder. The resulting monolithic pellets possess a unique anisotropic ordered structure which may exhibit further interesting, anisotropic

properties with respect to diffusion, thermal conductivity, and electrical conductivity. In this work, these high-density pellets are demonstrated to exhibit an anomalous gas densification property toward N<sub>2</sub>, and therefore a high H<sub>2</sub> storage capacity on a volumetric basis. Such high-density, graphene-like monoliths are expected to be promising for a variety of adsorbent applications related to energy storage and conversion.

## Author Contributions

**Atsushi Gabe:** Investigation, Writing - original draft. **Mohammed Ouzzine:** Investigation. **Erin E. Taylor:** Data curation. **Nicholas P. Stadie:** Methodology, data curation and review & editing. **Naoki Uchiyama:** Data curation. **Tomomi Kanai:** Data curation. **Yuta Nishina:** Data curation, Review & editing. **Hideki Tanaka:** Review & editing. **Zheng-Ze Pan:** Data curation. **Takashi Kyotani:** Conceptualization, review & editing. **Hiroto Nishihara:** Project administration, Writing - review & editing.

## Conflicts of interest

There are no conflicts to declare.

## Acknowledgements

This work was supported by JSPS KAKENHI (grant Nos. 17H01042 and 19H00913), the "Five-star Alliance" in "NJRC Mater. & Dev." and JST CREST (JPMJCR18R3).

## References

- M. Mohan, V. K. Sharma, E. A. Kumar and V. Gayathri, *Energy Storage*, 2019, 1, 1–26.
- D. Cazorla-Amorós, *Front. Mater.*, 2014, 1, 1–3.
- H. Nishihara, P. Hou, L. Li, M. Ito, M. Uchiyama, T. Kaburagi, A. Ikura, J. Katamura, T. Kawarada, K. Mizuuchi and T. Kyotani, *J. Phys. Chem. C*, 2009, 113, 3189–3196.
- D. J. Tranchemontagne, K. S. Park, H. Furukawa, J. Eckert, C. B. Knobler and O. M. Yaghi, *J. Phys. Chem. C*, 2012, 116, 13143–13151.
- R. J.-C. Dubey, T. Colijn, M. Aebli, E. E. Hanson, R. Widmer, K. V. Kravchuk, M. V. Kovalenko and N. P. Stadie, *ACS Appl. Mater. Interfaces*, 2019, 11, 39902–39909.
- K. Nomura, H. Nishihara, N. Kobayashi, T. Asada and T. Kyotani, *Energy Environ. Sci.*, 2019, 12, 1542–1549.
- K. Nomura, H. Nishihara, M. Yamamoto, A. Gabe, M. Ito, M. Uchimura, Y. Nishina, H. Tanaka, M. T. Miyahara and T. Kyotani, *Nat. Commun.*, 2019, 10, 1–10.
- H. Nishihara and T. Kyotani, *Chem. Commun.*, 2018, 54, 5648–5673.
- P. X. Hou, H. Orikasa, H. Itoi, H. Nishihara and T. Kyotani, *Carbon*, 2007, 45, 2011–2016.
- E. Masika and R. Mokaya, *Energy Environ. Sci.*, 2014, 7, 427–434.
- N. Balahmar, A. M. Lowbridge and R. Mokaya, *J. Mater. Chem. A*, 2016, 4, 14254–14266.
- E. E. Taylor, K. Garman and N. P. Stadie, *Chem. Mater.*, 2020, 32, 2742–2752.
- D. Lozano-Castelló, F. Suárez-García, Á. Linares-Solano and D. Cazorla-Amorós, in *Renewable Hydrogen Technologies*, eds. L. M. Gandía, G. Arzamendi and P. M. Diéguez, Elsevier, Amsterdam, 2013, pp. 269–291.
- N. Morimoto, H. Suzuki, Y. Takeuchi, S. Kawaguchi, M. Kunisu, C. W. Bielawski and Y. Nishina, *Chem. Mater.*, 2017, 29, 2150–2156.
- W. F. Watson, *Ind. Eng. Chem.*, 1955, 47, 1281–1286.
- F. Beckert, A. M. Rostas, R. Thomann, S. Weber, E. Schleicher, C. Friedrich and R. Mülhaupt, *Macromolecules*, 2013, 46, 5488–5496.
- M. Sohail Ahmad, H. Suzuki, C. Wang, M. Zhao and Y. Nishina, *J. Catal.*, 2018, 365, 344–350.
- H. Bi, T. Lin, F. Xu, Y. Tang, Z. Liu and F. Huang, *Nano Lett.*, 2016, 16, 349–354.
- H. Nishihara, H. Fujimoto, H. Itoi and K. Nomura, H. Tanaka, M. T. Miyahara, P. A. Bonnaud, R. Miura, A. Suzuki, N. Miyamoto, N. Hatakeyama, A. Miyamoto, K. Ikeda, T. Otomo and T. Kyotani, *Carbon*, 2018, 129, 854–862.
- H. Nishihara, Q. H. Yang, P. X. Hou, M. Unno, S. Yamauchi, R. Saito, J. I. Paredes, A. Martínez-Alonso, J. M. D. Tascón, Y. Sato, M. Terauchi and T. Kyotani, *Carbon*, 2009, 47, 1220–1230.
- Y. Li and R. T. Yang, *J. Phys. Chem. C*, 2007, 111, 11086–11094.
- H. Itoi, H. Nishihara, T. Kogure and T. Kyotani, *J. Am. Chem. Soc.*, 2011, 133, 1165–1167.
- M. Miyahara and K. E. Gubbins, *J. Chem. Phys.*, 1997, 106, 2865–2880.
- M. T. Kapelewski, T. Runčevski, J. D. Tarver, H. Z. H. Jiang, K. E. Hurst, P. A. Parilla, A. Ayala, T. Gennett, S. A. Fitzgerald, C. M. Brown and J. R. Long, *Chem. Mater.*, 2018, 30, 8179–8189.
- J. P. Marco-Lozar, M. Kunowsky, F. Suarez-Garcia, J. D. Carruthers and A. Linares-Solano, *Energy Environ. Sci.*, 2012, 5, 9833–9842.
- J. P. Marco-Lozar, M. Kunowsky, J. Donald Carruthers, A. Linares-Solano, *Carbon*, 2014, 76, 123–132.